Analyst

Accepted Manuscript

This article can be cited before page numbers have been issued, to do this please use: J. Wang, Y. Wang, S. Liu, H. Wang, X. Zhang, X. Song, J. Yu and J. Huang, *Analyst*, 2019, DOI: 10.1039/C9AN00316A.

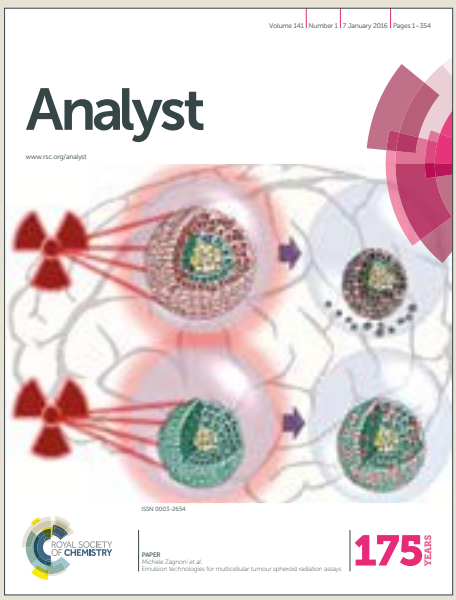

ROYAL SOCIETY OF CHEMISTRY

rsc.li/analyst

DOI: 10.1039/C9AN00316A

Primer remodeling amplification-activated multisite-catalytic hairpin assembly enabling concurrent formation of Y-shaped DNA nanotorches for fluorescent assay of ochratoxin A

Jingfeng Wang[a], Yu Wang[a], Su Liu[b], Haiwang Wang[a], Xue Zhang[a], Xiaolei Song[b], Jinghua Yu[c], Jiadong Huang[a c*]

a School of Biological Sciences and Technology, University of Jinan, Jinan 250022, P.R. China.

b School of Water Conservancy and Environment, University of Jinan, Jinan 250022, P.R. China.

c Key Laboratory of Chemical Sensing & Analysis in Universities of Shandong, School of Chemistry and Chemical Engineering, University of Jinan, Jinan 250022, P.R. China

*Corresponding Author.

E-mail: chm_huangjd@ujn.edu.cn; Tel.: +86-531-89736122; Fax: +86-531-82769122.

View Article Online
DOI: 10.1039/C9AN00316A

Abstract

DNA can be configured into unique high-order structures due to significantly high programmability such as three-way junctions-based structure (denoted Y-shaped DNA) for further application. Herein, we report a label-free fluorescent signal-on biosensor based on the target-driven primer remodeling rolling circle amplification (RCA)-activated multisite-catalytic hairpin assembly (CHA) enabling concurrent formation of Y-shaped DNA nanotorches (Y-DNTs) for ultrasensitive detection of ochratoxin A (OTA). Two kinds of masterly-designed probes termed Complex I and II are pre-prepared by the combination of circular template (CT) with OTA aptamer (S1), a substrate probe (S2) and hairpin probe 1 (HP1), respectively. Target OTA specifically binds to Complex I, resulting in the release of the remanent element in S2 and successive remodeling into mature primer for RCA by phi29 DNA polymerase, thus usable primer-CT complex is produced that actuates primary RCA. Then numerous Complex II can anneal with the first-generation RCA product (RP) with multiple sites for activating CHA process. With the participation of endonuclease IV (Endo IV) and phi29, HP1 as pre-primer containing a tetrahydrofuran abasic site mimic (AP site) in Complex II is converted into mature primer to initiate addition rounds of RCA. So, countless Y-DNTs are formed concurrently containing G-quadruplex structure that enables the *N*-methylmesoporphyrin IX (NMM) to be embedded, generating remarkably strong fluorescent signals. The biosensor is demonstrated to enable rapid and accurate detection of OTA with improved detection limit as low as 0.0002 ng mL^{-1} and widened dynamic range over 4 orders of magnitude featuring highly efficient and selective. Meanwhile, this method is proved to be capable for analyzing actual samples. Therefore,

View Article Online
DOI: 10.1039/C9AN00316A

this proposed strategy may establish a useful and practical platform for ultrasensitive detection of mycotoxin in food safety testing.

Keywords: fluorescent biosensor, rolling circle amplification, three-way junction, OTA detection, food analysis

View Article Online
DOI: 10.1039/C9AN00316A

Introduction

Ochratoxin (OT) is one kind of low molecular-secondary metabolites produced by *Aspergillus*, *Penicillium* fungi and other bacteria,[1] and belongs to the natural pollutants of mycotoxin group.[2] Typically, ochratoxin A (OTA) is the most toxic and widely distributed among mycotoxins, which can be found in crop production, processing and storage.[3, 4] Meanwhile, many studies have shown that OTA has nephrotoxicity, hepatotoxicity, embryonic toxicity, deformities, neurotoxicity, immunotoxicity, genetic toxicity and carcinogenicity.[5-7] The International Agency for Research on Cancer (IARC) has classified OTA as a possible human carcinogen based on substantial evidence of carcinogenicity found in several animal studies. Additionally, the United Nations Food and Agriculture Organization (FAO) estimates that approximately 25 percent of the world's grains are contaminated with mycotoxins.[8, 9] Due to the characteristics of OTA, such as trace, highly toxic and complicated pollution situation, the actual detection is quite difficult.

Currently, several typical methods have been applied for detection of OTA including high-performance liquid chromatography (HPLC),[10] HPLC-tandem mass spectrometry (HPLC-MS)[11] and immunoassay such as enzyme linked immunosorbent assay (ELISA).[12, 13] Nevertheless, the classical technologies suffered from the deficiency of high-cost, time-consuming, low sensitivity and poor repeatability in wide application. Thus, the establishment of sensitive and highly efficient detection methods is of great significance for the study of OTA pollution status, the effective reduction of its harm and the formulation of OTA limit standards in various actual samples. Up to now, aptasensors have been widely constructed for ultrasensitive detection of OTA via optical,[14, 15] electrochemical[16, 17] and other sensing platform,[18, 19] owing to aptamers'

significant specificity and affinity upon OTA.[20-22] Among all the biosensing technologies, fluorescent assay has been generally recognized as the superior candidates for widespread application taking advantages of rapidness, accuracy and high efficiency.[23-26] Not only that, label-free fluorescence strategies using fluorescent dyes like typical SYBR Green I or *N*-methylmesoporphyrin IX (NMM) with interaction-responsive emission have drawn more attention for further research due to facile design and low-cost.[27-29] Interestingly, it's characterized by a pronounced selectivity for DNA substrate exhibiting an attractive fluorescence signal enhancement.[30, 31]

Furthermore, with the purpose to improve the detection sensitivity, several isothermal amplification technologies such as strand displacement amplification (SDA),[32] palindromic sequence amplification (PSA),[33] catalytic hairpin assembly (CHA),[34] the loop-mediated isothermal amplification (LAMP)[35]recently have been employed into fluorescent assays. Except above, rolling circle amplification (RCA) has the unique superiority of simple design, high efficiency, straightforward operation for the fields of bioanalysis and nanotechnology.[36, 37] The RCA reaction can be actuated due to the high replication performance and the excellent continuous synthesis characteristics of DNA polymerase such as phi29 DNA polymerase, achieving an approximately 1000-fold to 10000-fold increase for linear amplification and producing a lot of reduplicated oligonucleotide sequences.[38-40] Notably, RCA products generally function as substrates via ingenious design for assembling with DNA probes.[41-43] In addition, catalytic hairpin assembly (CHA) as a promising and effective amplification strategy has proven to be an extraordinarily versatile tool for signal conversion.[44-47] Hence, we have developed a label-free fluorescent assay for OTA determination based on the target-driven primer remodeling RCA-activated multisite-CHA dual signal amplification concurrent strategy.

The "primer remodeling" process is carried out as follows: Due to the phi29 DNA polymerase with 3'-5' exonuclease activity, the mismatched element of S2 can be remodeled into mature primer for first-run RCA after the combination of OTA and aptamer. Meanwhile, the primer-generation process is extremely robust via Endo IV-catalyzed cyclic cleavage of HP1, and the mismatched element of HP1 against CT was remodeled into mature primer for second-run RCA. Therefore, the proposed strategy may establish a robust and high efficient biosensing platform for ultrasensitive detection of OTA.

2. Materials and methods

2.1 Materials and reagents

All DNA oligonucleotides sequences listed in **Table 1** were purified by HPLC and synthesized by Sangon Biotechnology Co. Ltd. (Shanghai, China). Ochratoxin A (OTA), Zearalenone (ZEN) were purchased from Aladdin Biochemical Technology Co. Ltd. (Shanghai, China). Aflatoxin B1 (AFB1) was obtained from Sigma-Aldrich (Shanghai, China). T4 DNA ligase, 10×T4 DNA ligase reaction buffer (50 mM Tris-HCl, 10 mM $MgCl_2$, 10 mM DTT, 1 mM ATP, pH 7.5), *E. coli* exonuclease I (Exo I), *E. coli* exonuclease III (Exo III), phi29 DNA polymerse, 10×phi29 DNA polymerse reaction buffer (50 mM Tris-HCl, 10 mM $MgCl_2$, 10 mM $(NH_4)_2SO_4$, 4 mM DTT, pH 7.5), deoxynucleotide (dNTP) solution mix, endonuclease IV (Endo IV) were purchased from New England Biolabs (Ipswich, MA, USA). N-methyl mesoporphyrin IX (NMM) was purchased from Frontier& Scientific (Philadelphia, United States). The stock solution of NMM (5 μM) was prepared in dimethyl sulfoxide (DMSO), stored in darkness at -20℃. The concentration of NMM was measured by UV-vis spectrometer (Shimadzu UV-2600, Japan) and found to be λ=379 nm, assuming an extinction coefficient of

1.45×10^5 M^{-1} cm^{-1}. The agarose and DNA marker (DL 15000) were purchased from Takara Biotechnology Co. Ltd. (Dalian, China). Other chemicals were of analytical grade and were used without further purification. Ultrapure water obtained from a Millipore filtration system was used throughout.

Table 1 DNA oligonucleotides sequence used in this work

Oligonucleotides name	Sequence (5' to 3')
S1	GATCGGGTGTGGGTGGCGTAAAGGGAGCATCGGACAT TTTTT-inverted dT
S2	GATATCAGCGATGGCCGATGCTTTTTTTCACCCGATC
padlock probe	P-CTGATATCCGTCCCTGGGTAGAGACTGGACGTCCCTG GGTAGAGACTGGACCATCG
ligation probe	ACGGATATCAGCGATGGTCCAGT
HP1	GATATCAGCGATGGGTAXCGGCTTGAGATGTTAGGGAC GAGTGCGCACTCCACAAGGCACTCGTCCCT**GGGTGGG T**-inverted dT
HP2	**GGGTGGGT**CTTGTGGAGTGCGCTTGAGATGTTGCACT CGTCCCTAACATCTCAAGCCGTTACTTTTTT-inverted dT
HP3	**GGGTGGGT**AGGGACGAGTGCCTTGTGGAGTGCGCACG TGCAACATCTCAAGCGCACTCCACAAG**GGGTGGGT**-inverted dT

The sequence underlined in the S1 is the aptamer of OTA. The 3' inverted dT modification in S1, HP1, HP2 and HP3. The P in the padlock probe denotes a 5' phosphate modification. The X highlighted in red denotes the tetrahydrofuran abasic site mimic (AP site). G-rich sequences in bold in HP1, HP2 and HP3 represent half-baked G-quadruplex structure without assembly.

2.2 Apparatus

Gel electrophoresis was conducted using DYCZ-24DN electrophoresis cell (LIUYI, Beijing, China) and Bio-Rad Gel imaging system (Bio-Rad, USA). Gel electrophoresis was conducted using DYCZ-24DN electrophoresis cell (LIUYI, Beijing, China) and

Bio-Rad Gel imaging system (Bio-Rad, USA). Fluorescence spectra were recorded using an Agilent Cary Eclipse spectrofluorometer (Hitachi, Japan) with excitation at 399 nm. The slit was set to be 10 nm for both the excitation and the emission.

2.3 Preparation of circular template

After an intramolecular ligation in an aliquot of 60 μL reaction system, the circular template was prepared. It means that 6 μL of 100 μM 5'-phosphorylated linear padlock probe, 6 μL of 100 μM ligation probe, 6 μL 10×T4 DNA ligase reaction buffer (50 mM Tris-HCl, 10 mM $MgCl_2$, 10 mM DTT, 1 mM ATP, pH 7.5) were added and incubated for initial denaturation at 95 ℃ for 5 min, then slowly cooled down to room temperature. Immediately, 3 μL of 400 U μL^{-1} T4 DNA ligase was added and incubated at 16 ℃ overnight. The ligation reaction solution was terminated by a thermal treatment at 65 ℃ for 10 min to inactivate the T4 DNA ligase. After that, to digest the unnecessary bases, 1 μL Exo I, 2 μL Exo III were added to the solution above followed by incubation 2 h at 37 ℃. After the exonucleases were deactivated at 85 ℃, the resultant products were stored at 4 ℃ for further use.

2.4 Preparation of complex probe

Two different complex probes were prepared via a hybridization reaction. Firstly, the Complex I was prepared in an aliquot of 50 μL reaction system containing 25 μL of 10 μM circular template, 2.5 μL of 100 μM arch probe, 2.5 μL of 100 μM OTA-aptamer, 10 μL 5×PBS buffer (10 mM Na_2HPO_4, 10 mM NaH_2PO_4, 140 mM NaCl, 1 mM KCl, 1 mM $MgCl_2$, 1 mM $CaCl_2$, pH=7.4) which were added and incubated for initial denaturation at 37 ℃ for 1 h. Likewise, the Complex II was prepared via the process of DNA assembly containing 5 μL of 10 μM circular template, 5 μL of 10 μM HP1, 10 μL 5×PBS buffer.

View Article Online
DOI: 10.1039/C9AN00316A

2.5 Detection of OTA

The detailed procedure was as follows: 3 μL of 1 μM Complex I, 3 μL of 5 μM Complex II, 3 μL of 5 μM HP2 and 3 μL of 5 μM HP3 were added into 30 μL of reaction mixture containing 3 μL 10×phi29 DNA polymerase reaction buffer (50 mM Tris-HCl, 10 mM $MgCl_2$, 10 mM $(NH_4)_2SO_4$, 4 mM DTT, pH 7.5), 3 μL of 10 $U \cdot \mu L^{-1}$ phi29 DNA polymerase, 1.5 μL of 10 $U \cdot \mu L^{-1}$ Endo IV, 1.5 μL of 10 mM dNTPs, 3 μL of 5 μM NMM and 3 μL of different concentrations of OTA, which were incubated at 37 ℃ for 90 min. Ultimately, the above reaction solution was mixed with 70 μL of ultrapure water and scanned using Agilent Cary Eclipse spectrofluorometer. Unless noted otherwise, all experiments for OTA measurements were repeated three times in this research.

2.6 Gel Electrophoresis

The gel electrophoresis was demonstrated to analyze the preparation of the circular template and target-activated RCA reaction products on a 1% agarose gel in 50 mM Tris-borate running buffer (2 mM EDTA, pH=8.2) at 145 V for 35 min. Then the resultant product was visualized using a Bio-Rad Gel imaging system after electrophoresis.

2.7 Analysis of OTA in Actual Samples

Red wine was chosen as the actual sample for various concentrations of OTA assay. Before analysis, sediments in the red wine samples were removed via filtration process. Subsequently, the actual samples were adjusted to pH=7.4 approximately and diluted 20-fold for the further research. A range of various concentrations (0.1, 0.5, 1, 5, 10 ng mL^{-1}) were spiked into the samples gaining standard samples. The subsequent manipulations were identical with the above sections.

View Article Online
DOI: 10.1039/C9AN00316A

3. Results and discussion

3.1 Principle of the proposed fluorescence biosensing strategy

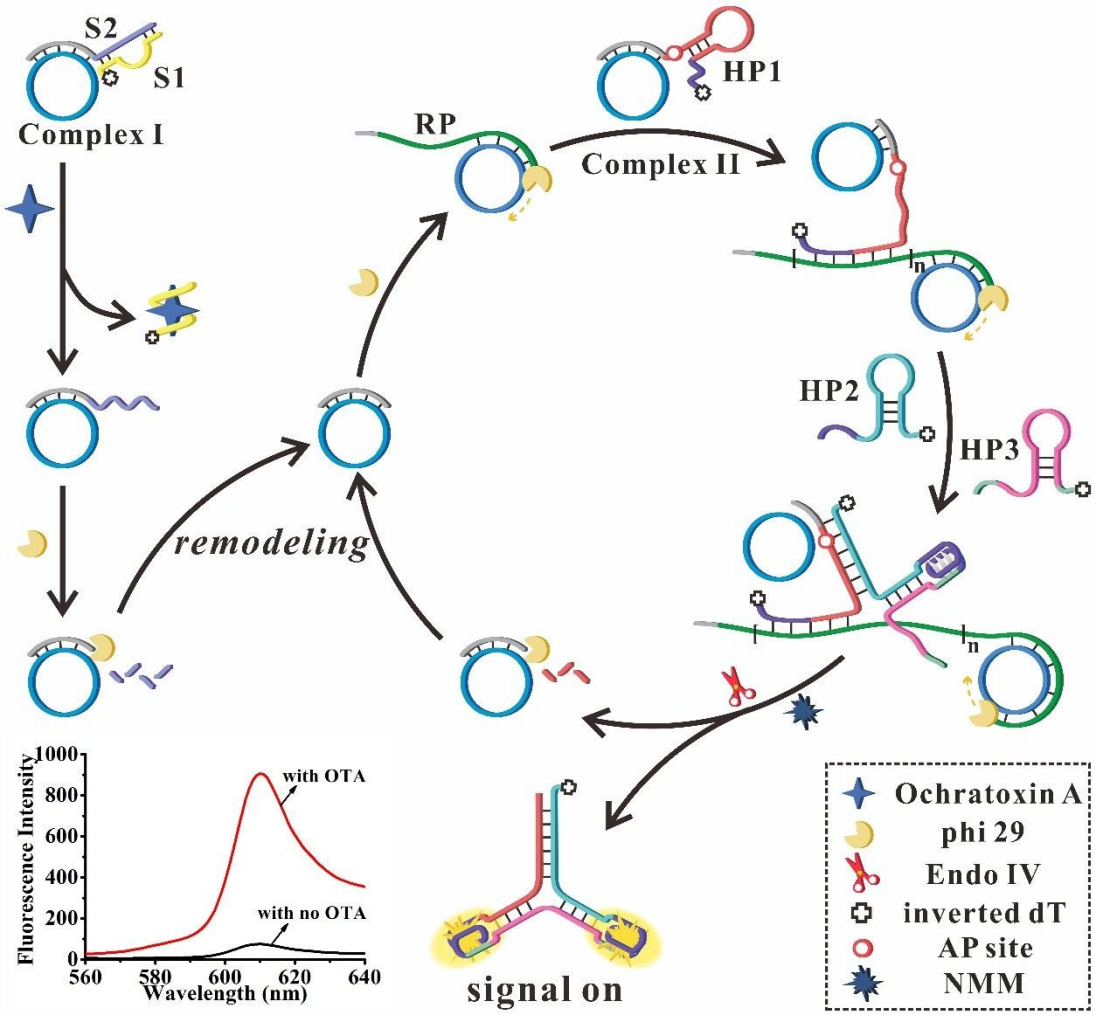

Scheme 1. Schematic illustration on the label-free fluorescent signal-on sensing platform for ultrasensitive detection of OTA based on the target-driven primer remodeling RCA-activated multisite-CHA dual signal amplification concurrent strategy.

Scheme 1 depicts the working principle of the proposed strategy for ultrasensitive detection of OTA. Typically, aptamer structure-switching concept can be implemented for RCA process through the facile design of a switchable DNA assembly namely as Complex I made of a circular template (CT), OTA aptamer (S1) and a substrate probe (S2) which as the pre-primer binding with both S1 and CT. In the presence of OTA,

OTA binding to the S1 releases the remanent element of S2, resulting unpaired nucleotides that can be remodeling into mature primer for RCA by phi29 DNA polymerase. The phi29 DNA polymerase can trigger the hydrolyzation reaction against the mismatched bases due to its 3'-5' exonuclease activity,[48, 49] converting the free stretching 3' terminus of S2 into the mature RCA primer. Immediately, the trimming products of amplifiable Complex I were converted into the first-generation RCA under the action of phi29 and dNTPs, achieving the first-generation of RCA products (RP) with multiple sites for initiating CHA process. Additionally, two split G-quadruplex sequences were respectively integrated into a pair of DNA hairpin probes (HP1, HP2 and HP3) which were facile-designed. Whereas, Complex II was ingenious-designed and pre-prepared by hybridizing CT with HP1 containing a tetrahydrofuran abasic site mimic (AP site) for achieving feeding back into second-run RCA process. The spontaneous hybridization reaction among Complex II, HP2 and HP3 was kinetically inhibited owing to the complementary sequences were blocked in the stems. Whereafter, the hairpin structure of HP1 was opened specifically by the first-generation of RP, and the 3'-termini of HP1 could bind with RP forming the briefly intermediate structure. The newly exposed part of HP1 could hybridize with the sticky end of HP2 with the formation of short-life intermediate RP-HP1-HP2 complexes resulting in the cleavage of AP sites embedded in duplexes via Endo IV, followed by the detachment of residuary Complex II forming RP-HP1-HP2 complexes. The rest of Complex II with exposed stretching 3' terminus was then remodeled and converted into a mature primer for feeding back into the second-run RCA. Furthermore, numerous second-generation RP can combine with an increasing number of Complex II resulting in countless AP sites are cleaved owing to highly efficient exponential RCA-activated CHA reaction. Finally,

Y-shaped DNA nanotorches (Y-DNTs) are obtained through CHA process and bring the two split G-quadruplex fragments into close-enough proximity resulting in the formation of the intact G-quadruplex structures which used as signal-transducing units to enhance the fluorescence signal output of the NMM expressly. On the contrary, in the absence of OTA, the primary RCA reaction can be well-inhibited owing to the facile design of S1-S2 hybridization structure generating a negligible fluorescent signal. Therefore, our developed biosensor based on the target-driven primer-remodeling RCA-activated CHA dual-amplification strategy establishing a potential platform for detecting OTA featuring highly sensitive and specific in food analysis.

3.2 Feasibility Investigation OTA Assay

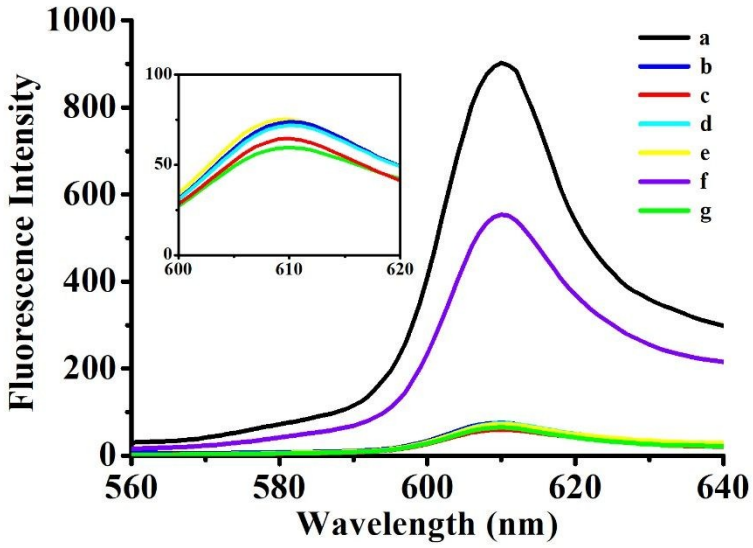

Fig.1 Fluorescence emission spectra responses of this biosensor obtained upon analyzing 10 ng mL^{-1} OTA (curve a). Curves (b to g) are for the feasibility research of the strategy which is controlled with no OTA (curve b), no Complex II (curve c), no HP3 (curve d), no phi29 (curve e), no Endo IV (curve f) and non-target AFB1 in place of OTA (curve g).

To check the feasibility of the proposed strategy, several fluorescence emission spectra responses were obtained upon analyzing OTA under mixture conditions shown in **Fig.1**. In the presence of 10 ng mL^{-1} OTA, a significantly strong emission peak was obtained at 610 nm approximately, indicating numerous Y-DNTs were generated and the NMM was embedded in G-quadruplex structure with a remarkably enhancement of fluorescent signal, which was attributed to target-driven primer-remodeling RCA-activated CHA dual-amplification. Contrarily, in the absence of OTA, there was a negligible fluorescent signal at 610 nm (curve b), implying that the primary RCA was inhibited. Without the participation of Complex II and HP3 in CHA process, the CHA reaction was almost well-inhibited resulting in producing weak fluorescence emission responses (curve c and d). When phi29 was absent in the reaction process, it was observed that the fluorescence peak was inappreciable (curve e) due to the RCA reaction was canceled. Moreover, a slightly weaker fluorescence intensity was obtained in the absence of Endo IV (curve f), implying that Endo IV played a significant role in achieving feeding back into second-run RCA process. Additionally, the replacement from non-target AFB1 to OTA, there was an inappreciable fluorescence emission peak, demonstrating our developed method was carried out only by OTA with high selectivity. Additionally, Straightforward proof of the reaction principle and the RCA-initiated CHA process via gel electrophoresis were illustrated in **Fig.S1**. These results above obtained clearly exhibited that our proposed strategy based on the OTA-driven primer remodeling RCA-activated multisite-CHA dual amplification strategy can provide a feasible platform for the ultrasensitive detection of OTA.

3.3 Gel Electrophoresis Characterization

View Article Online
DOI: 10.1039/C9AN00316A

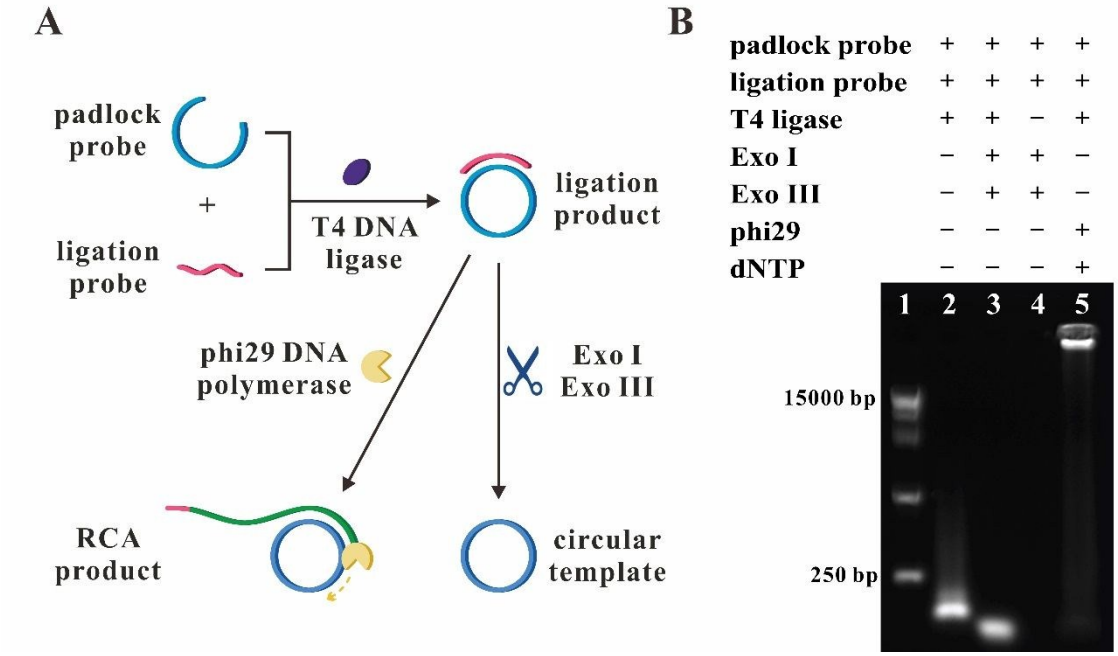

Fig.2 (A) Schematic illustration of ligation process and RCA reaction. (B) Gel electrophoresis characterization image.

Straightforward proof of the ligation reaction and RCA reaction were verified via gel electrophoresis and the results were depicted in **Fig.2**. The synthesis process of circular template was described in detail in **Fig.2A**. As shown in **Fig. 2B**, lane 1 was on behalf of the DNA marker, and lane 2 displayed the ligase reaction that the padlock probe could be cyclic after hybridization with the ligation probe and specifically ligated in the aid of T4 DNA ligase generating a bright band. Moreover, a bright band were obtained after adding Exo I and Exo III remaining only the circular template as shown in lane 3. Nevertheless, no band appeared on the figure in the absence of T4 DNA ligase after the incubation of padlock probe and ligation probe, illustrating the both probes were digested by exonuclease (lane 4). The above results fully demonstrate that the circular template can be successfully prepared for the following reactions. As seen from lane 5, a bright band with the large-molecule-weight RCA product and extremely low mobility

was appeared on the image, illustrating RCA reaction was commendably implemented and the high efficiency of RCA reaction.

3.4 Optimization of The Experimental Conditions

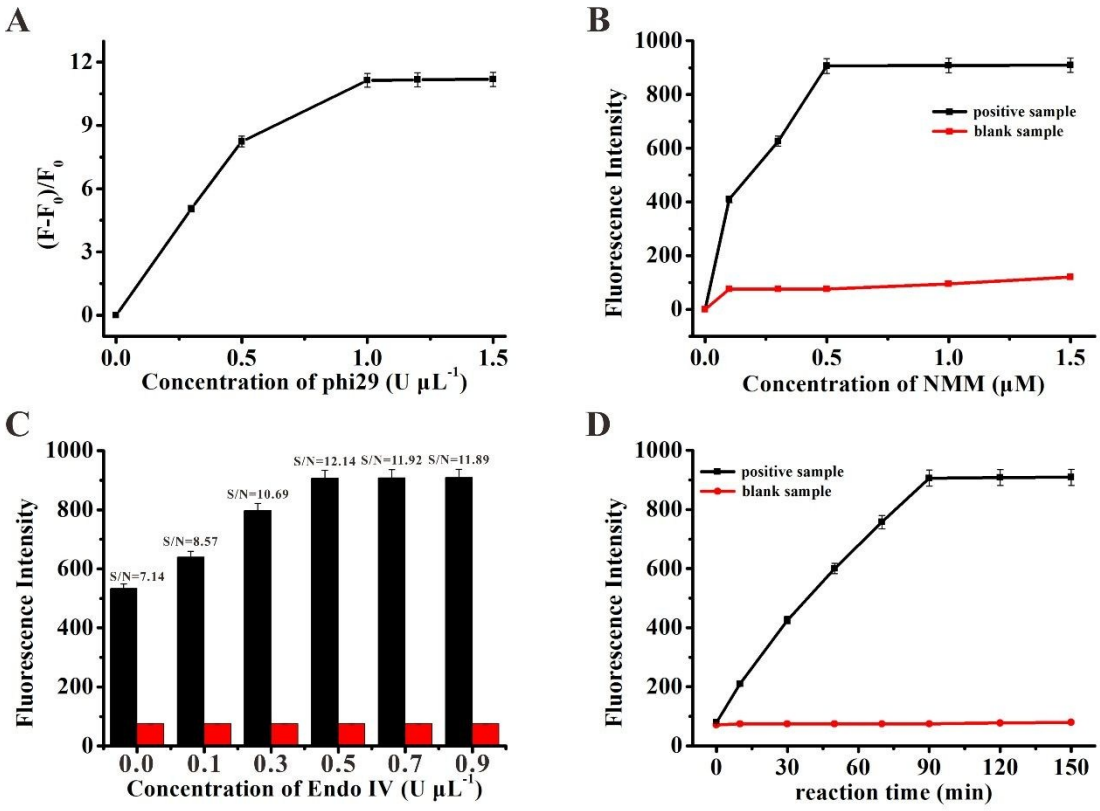

Fig.3 (A) Effect of the concentration of phi29 on the fluorescence emission peak of the biosensor; (B) Effect of the concentration of NMM on the fluorescence emission peak of the biosensor in the presence and absence of 10 ng mL^{-1} OTA; (C) Effect of the concentration of Endo IV on the fluorescence emission peak of the biosensor in the presence and absence of 10 ng mL^{-1} OTA; (D) Effect of the reaction time on the fluorescence emission peak of the biosensor in the presence and absence of 10 ng mL^{-1} OTA. Error bars are standard deviations across thrice repetitive experiments.

In order to achieve the perfect analytical performance of the proposed strategy, a series of experimental conditions including the concentration of phi29 DNA polymerase, NMM and Endo IV, the reaction time were successively investigated. Firstly, **Fig.3A**

depicts the $(F-F_0)/F_0$ value (F and F_0 represent the fluorescence emission peak intensity at 610 nm in the presence and absence of 10 ng mL^{-1} OTA respectively) gradually increases with the aid of phi29 DNA polymerase concentration and reaches equilibrium with the optimal concentration of 1 U μL^{-1}. Secondly, as shown in **Fig.3B**, the fluorescence intensities increase with the increasing dosage of NMM until the concentration reached 0.5 μM. Besides, Endo IV is of great significance in feedback amplification and a favorable performance is obtained under the optimal concentration of 0.5 U μL^{-1} (**Fig. 3C**). At last but not least, the growth trend of reaction time for the proposed strategy flattened out at 90 min as shown in **Fig. 3D**. These results above lay the foundation of further assay.

3.5 Analytical Performance of OTA Assay

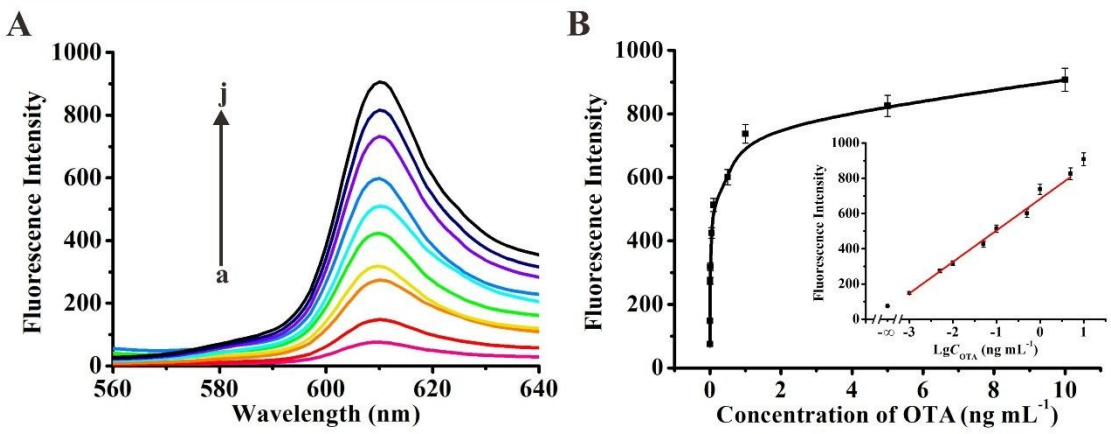

Fig.4 (A) Fluorescent emission responses upon the different concentration of OTA (from curve a to j: 0, 1×10^{-3}, 5×10^{-3}, 1×10^{-2}, 5×10^{-2}, 1×10^{-1}, 5×10^{-1}, 1, 5 and 10 ng mL^{-1}). (B) Relationship between the fluorescence intensity and the concentration of OTA. The inset depicts calibration curve of fluorescence intensity at 610 nm upon different concentrations. Error bars are standard deviations across three parallel experiments.

Moreover, the perfect analytical performance of our developed biosensor towards OTA was investigated under the optimal experimental conditions, of which the results

generation by fluorescence spectroscopy were depicted in **Fig.4**. As shown precisely in **Fig. 4A**, the normalized fluorescence intensities increased significantly with the advance of OTA concentration from 1×10^{-3} to 10 ng mL^{-1} over 4 orders of magnitude. The curve responses to different OTA concentration was plotted in Fig. 4B, and inset depicts a favorable linear relationship between the fluorescence intensities and the logarithmic concentration of OTA with a regression equation of $F=694.1+185.7\times\lg C_{OTA}$ and a correlation coefficient (R^2) of 0.9934. In terms of the 3σ rule, the limit of detection (LOD) was calculated to be 0.0002 ng mL^{-1} which is comparable to or better than those of the most reported detection methods upon OTA listed in **Table S1**. Therefore, our developed method exhibits improved sensitivity and widened dynamic range owing to highly efficient RCA-activated multisite CHA dual-amplification strategy.

3.6 Validation Assay of Specificity

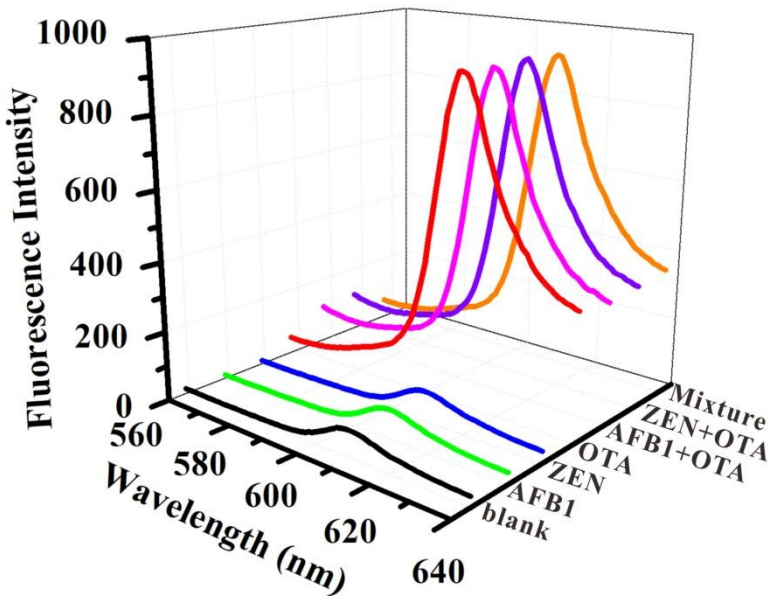

Fig.5 Fluorescent responses to the different mycotoxins. The concentration of OTA is 10 ng mL^{-1}. The concentration of the non-target is 50 ng mL^{-1}. Mixture represents the mix of AFB1, ZEN and OTA.

View Article Online
DOI: 10.1039/C9AN00316A

In order to evaluate the specificity of the developed biosensor for the ultrasensitive detection of OTA, several fluorescent responses upon other interferences (AFB1, ZEN and mixture) were measured as controls. As shown in **Fig.5**, significantly strong fluorescence signals were observed only in the presence of OTA due to the specific recognition and strong combining capability of aptamer toward target OTA, which was indicated that fluorescence signals obtained upon OTA are not interfered by the presence of other mycotoxins in the mixture. Therefore, these results above indicate that our proposed strategy indeed establish a significant platform for OTA quantification with high specificity in food analysis.

3.7 Determination of OTA in Actual Samples

We further measure the OTA in actual red wine samples for deep validation and reliability of our proposed strategy. The red wine samples were spiked with 5 different concentrations of OTA (0.1, 0.5, 1, 5, 10 ng mL^{-1}) and analyzed through our fluorescence assay. As depicted in **Table 2**, the resultant recoveries range from 96.04-102.2% and relative standard deviation (RSD) in the range of 0.16-1.18%, and they show a good agreement with the determination by HPLC. Thus, the developed biosensor may establish a platform for ultrasensitive detection of OTA in actual samples with a significantly favorable reliability.

Table 2 Application of our proposed method for the determination of OTA in red wine samples and comparison with HPLC

Actual Sample	Spiked amount (ng mL^{-1})	Developed method (±SD, n=5)	HPLC (±SD, n=5)	RSD (%)	Recovery (%)
sample 1	10	9.872±0.005	9.864±0.062	0.63	98.64
sample 2	5	4.980±0.012	4.977±0.008	0.16	99.54
sample 3	1	0.9792±0.024	0.9748±0.009	0.97	97.48

sample 4	0.5	0.5046±0.017	0.5108±0.009	1.81	102.2
sample 5	0.1	0.09617±0.021	0.09604±0.002	1.71	96.04

4. Conclusion

In summary, we construct a facile and highly efficient label-free fluorescent biosensor for ultrasensitive detection of OTA based on primer remodeling RCA-activated multisite-CHA enabling concurrent formation of Y-DNTs. The proposed strategy mainly features with several significant aspects. Above all, aptamer structure-switching concept can be implemented for RCA process through the facile design of a switchable DNA assembly namely as Complex I. Thus, OTA binding to the aptamer releases the aptamer-binding element triggering primer remodeling owing to phi29 DNA polymerase, featuring high amplification efficiency and excellent selectivity. Secondly, the RCA products as the promoter of CHA can provide multisite that can combine with ingenious-designed Complex II achieving concurrent duplex-amplification reaction. Thirdly, Y-DNTs are obtained through CHA process and bring the two split G-quadruplex fragments into close-enough proximity enabling formation of the intact G-quadruplex structures used as signal-transducing units to enhance the fluorescence signal output of the NMM expressly. Moreover, this approach has demonstrated to enable accurate determination of OTA with improved detection limit as low as 0.0002 ng mL^{-1} and widened dynamic range over 4 orders of magnitude, and this method is proved to be capable for analyzing actual samples. Hence, our concurrent duplex-amplification strategy indeed exhibits favorable applications in detection of mycotoxins with high sensitivity and specificity, possessing enormous potential in food safety testing.

Acknowledgements

This work was supported by National Natural Science Foundation of China (31471644), the Primary Research & Development Plan of Shandong Province (2017GSF220009), the Program for Taishan Scholer of Shandong Province (ts201712048).

References

1. J. W. Bennett and M. Klich, *Clinical microbiology reviews*, 2003, **16**, 497-516.
2. H. S. Hussein and J. M. Brasel, *Toxicology*, 2001, **167**, 101-134.
3. K. J. van der Merwe, P. S. Steyn, L. Fourie, D. B. Scott and J. J. Theron, *Nature*, 1965, **205**, 1112-1113.
4. R. Velu and M. C. DeRosa, *Analyst*, 2018, **143**, 4566-4574.
5. A. Pfohl-Leszkowicz and R. A. Manderville, *Molecular nutrition & food research*, 2007, **51**, 61-99.
6. M. E. Bezeria da Rocha, F. d. C. Oliveira Freire, F. B. Feitosa Maia, M. I. Florindo Guedes and D. Rondina, *Food Control*, 2014, **36**, 159-165.
7. M. E. Flores-Flores, E. Lizarraga, A. L. de Cerain and E. Gonzalez-Penas, *Food Control*, 2015, **53**, 163-176.
8. V. Ostry, F. Malir, J. Toman and Y. Grosse, *Mycotoxin Research*, 2017, **33**, 65-73.
9. S. Marin, A. J. Ramos, G. Cano-Sancho and V. Sanchis, *Food and Chemical Toxicology*, 2013, **60**, 218-237.
10. C. Giovannoli, C. Passini, F. Di Nardo, L. Anfossi and C. Baggiani, *Journal of Agricultural and Food Chemistry*, 2014, **62**, 5220-5225.
11. K. F. Nielsen, A. F. Ngemela, L. B. Jensen, L. S. de Medeiros and P. H. Rasmussen, *Journal of Agricultural and Food Chemistry*, 2015, **63**, 1029-1034.
12. B.-H. Liu, Z.-J. Tsao, J.-J. Wang and F.-Y. Yu, *Analytical chemistry*, 2008, **80**, 7029-7035.
13. L. Barthelmebs, J. Jonca, A. Hayat, B. Prieto-Simon and J.-L. Marty, *Food Control*, 2011, **22**, 737-743.
14. S. Wu, N. Duan, X. Ma, Y. Xia, H. Wang, Z. Wang and Q. Zhang, *Analytical Chemistry*, 2012, **84**, 6263-6270.

15. L. Lv, C. Cui, C. Liang, W. Quan, S. Wang and Z. Guo, *Food Control*, 2016, **60**, 296-301.
16. T. Liang, G. Sun, L. Cao, J. Li and L. Wang, *Food Hydrocolloids*, 2019, **87**, 858-868.
17. W. Chen, C. Yan, L. Cheng, L. Yao, F. Xue and J. Xu, *Biosensors & Bioelectronics*, 2018, **117**, 845-851.
18. D. Song, R. Yang, S. Fang, Y. Liu, F. Long and A. Zhu, *Microchimica Acta*, 2018, **185**.
19. M. Majdinasab, M. Sheikh-Zeinoddin, S. Soleimanian-Zad, P. Li, Q. Zhang, X. Li, X. Tang and J. Li, *Food Control*, 2015, **47**, 126-134.
20. J. A. Cruz-Aguado and G. Penner, *Journal of agricultural and food chemistry*, 2008, **56**, 10456-10461.
21. J. Chi, M. Chen, L. Deng, X. Lin and Z. Xie, *Analyst*, 2018, **143**, 5210-5217.
22. C. Song, W. Hong, X. Zhang and Y. Lu, *Analyst*, 2018, **143**, 1829-1834.
23. K. Wu, C. Ma, H. Zhao, M. Chen and Z. Deng, *Food Chemistry*, 2019, **277**, 273-278.
24. D. Song, R. Yang, S. Fang, Y. Liu and F. Long, *Microchimica Acta*, 2018, **185**.
25. S. Lv, Y. Tang, K. Zhang and D. Tang, *Analytical Chemistry*, 2018, **90**, 14121-14125.
26. Z. Qiu, J. Shu and D. Tang, *Analytical Chemistry*, 2017, **89**, 5152-5160.
27. A. G. Wang, T. Dong, H. Mansour, G. Matamoros, A. L. Sanchez and F. Li, *Acs Sensors*, 2018, **3**, 205-210.
28. M.-Q. He, K. Wang, W.-J. Wang, Y.-L. Yu and J.-H. Wang, *Analytical Chemistry*, 2017, **89**, 9292-9298.
29. Y. Guo, Q. Chen, Y. Qi, Y. Xie, H. Qian, W. Yao and R. Pei, *Biosensors & Bioelectronics*, 2017, **87**, 320-324.
30. F. Geng, X. Jiang, Y. Wang, C. Shao, K. Wang, P. Qu and M. Xu, *Sensors and Actuators B-Chemical*, 2018, **260**, 793-799.
31. J. Ren, J. Wang, J. Wang, N. W. Luedtke and E. Wang, *Biosensors & Bioelectronics*, 2012, **31**, 316-322.
32. Z. Huang, Z. Luo, J. Chen, Y. Xu and Y. Duan, *Acs Sensors*, 2018, **3**, 2423-2431.

33. R. Zeng, Z. Luo, L. Su, L. Zhang, D. Tang, R. Niessner and D. Knopp, *Analytical Chemistry*, 2019, **91**, 2447-2454.
34. R. Zeng, Z. Luo, L. Zhang and D. Tang, *Analytical Chemistry*, 2018, **90**, 12299-12306.
35. B. Tian, J. Ma, T. Z. G. de la Torre, A. Balint, M. Donolato, M. F. Hansen, P. Svedlindh and M. Stromberg, *Acs Sensors*, 2016, **1**, 1228-1234.
36. G. D. Hamblin, K. M. M. Carneiro, J. F. Fakhoury, K. E. Bujold and H. F. Sleiman, *Journal of the American Chemical Society*, 2012, **134**, 2888-2891.
37. X. Liu, M. Song, T. Hou and F. Li, *Acs Sensors*, 2017, **2**, 562-568.
38. W. Zhao, M. M. Ali, M. A. Brook and Y. Li, *Angewandte Chemie (International ed. in English)*, 2008, **47**, 6330-6337.
39. S. Wang, Y. Ji, H. Fu, H. Ju and J. Lei, *Analyst*, 2019, **144**, 691-697.
40. E. Xiong and L. Jiang, *Analyst*, 2019, **144**, 634-640.
41. J. Wang, Y. Wang, S. Liu, H. Wang, X. Zhang, X. Song and J. Huang, *Analyst*, 2018, **143**, 3951-3958.
42. X. Tang, R. Deng, Y. Sun, X. Ren, M. Zhou and J. Li, *Analytical Chemistry*, 2018, **90**, 10001-10008.
43. S. Liu, H. Fang, C. Sun, N. Wang and J. Li, *Analyst*, 2018, **143**, 5137-5144.
44. X. Li, J. Xie, B. Jiang, R. Yuan and Y. Xiang, *Acs Applied Materials & Interfaces*, 2017, **9**, 5733-5738.
45. X. Peng, W.-B. Liang, Z.-B. Wen, C.-Y. Xiong, Y.-N. Zheng, Y.-Q. Chai and R. Yuan, *Analytical Chemistry*, 2018, **90**, 7474-7479.
46. E. Xiong, X. Yan, X. Zhang, Y. Li, R. Yang, L. Meng and J. Chen, *Analyst*, 2018, **143**, 2799-2806.
47. L. Ge, W. Wang, T. Hou and F. Li, *Biosensors & Bioelectronics*, 2016, **77**, 220-226.
48. C. Garmendia, A. Bernad, J. A. Esteban, L. Blanco and M. Salas, *The Journal of biological chemistry*, 1992, **267**, 2594-2599.
49. M. de Vega, J. M. Lazaro, M. Salas and L. Blanco, *Journal of molecular biology*, 1998, **279**, 807-822.